GIFTS SM EDU Radiometric and Spectral Calibrations

J. Tian [a,*], R. A. Reisse [b], D. G. Johnson [c], M. J. Gazarik [c]

[a] SSAI, MS 468, NASA Langley Research Center, Hampton, VA 23681-2199 – j.tian@larc.nasa.gov
[b] MS 434, NASA Langley Research Center, Hampton, VA 23681-2199 – robert.a.reisse@nasa.gov
[c] MS 468, NASA Langley Research Center, Hampton, VA 23681-2199– (david.g.johnson, michael.j.gazarik)@nasa.gov

Abstract – The Geosynchronous Imaging Fourier Transform Spectrometer (GIFTS) Sensor Module (SM) Engineering Demonstration Unit (EDU) is a high resolution spectral imager designed to measure infrared (IR) radiance using a Fourier transform spectrometer (FTS). The GIFTS instrument gathers measurements across the long-wave IR (LWIR), short/mid-wave IR (SMWIR), and visible spectral bands. The raw interferogram measurements are radiometrically and spectrally calibrated to produce radiance spectra, which are further processed to obtain atmospheric profiles via retrieval algorithms. This paper describes the processing algorithms involved in the calibration. The calibration procedures can be subdivided into three categories: the pre-calibration stage, the calibration stage, and finally, the post-calibration stage. Detailed derivations for each stage are presented in this paper.

Keywords: Remote sensing; Fourier transform spectrometry; Geosynchronous Imaging Fourier Transform Spectrometer (GIFTS); interferogram processing; radiometric calibration.

1. INTRODUCTION

The Geosynchronous Imaging Fourier Transform Spectrometer (GIFTS) Sensor Module (SM) Engineering Demonstration Unit (EDU) is a high resolution spectral imager designed to measure infrared (IR) radiance using a Fourier transform spectrometer (FTS). The GIFTS instrument employs three Focal Plane Arrays (FPAs), which gather measurements across the long-wave (685-1130 cm^{-1}) IR (LWIR), short/mid-wave (1650-2250 cm^{-1}) IR (SMWIR), and visible spectral bands (Best, 2001). The raw interferogram measurements are radiometrically and spectrally calibrated to produce radiance spectra, which are further processed to obtain atmospheric profiles via retrieval algorithms.

The calibration procedures can be subdivided into three categories. In the pre-calibration stage, a phase correction algorithm is applied to the decimated and filtered complex interferogram. The resulting imaginary part of the spectrum contains only the noise component of the uncorrected spectrum. The phase correction operation is performed on a set of interferogram scans for the ambient, hot blackbody references, and scene measurements. In the calibration stage, we first compute the spectral responsivity based on the previous results, from which, the calibrated ambient blackbody (ABB), hot blackbody (HBB), and scene spectra can be obtained. In the post-calibration stage, we estimate the Noise Equivalent Spectral Radiance (NESR) from the calibrated ABB and HBB spectra. We then implement a correction scheme that compensates for the effects of fore-optics. The FPA off-axis effect correction technique also is presented.

2. CALIBRATION ALGORITHMS

2.1 Pre-calibration Procedures

In the pre-calibration stage, a phase correction algorithm is applied to the decimated and filtered complex interferogram $I_m(n)$. Its complex spectrum $N_m(\sigma)$ has the form of

$$N_m(\sigma) = N(\sigma)e^{j\phi(\sigma)} + n(\sigma), \quad (1)$$

where $n(\sigma)$ is the noise vector, and $N(\sigma)$ is the real and noise-free spectrum. To estimate and correct the phase function $\phi(\sigma)$, we adopt the Forman-Vanesse-Steel (FVS) method (Forman, 1966). In this algorithm, a Hamming window $w(n)$ is first applied to the complex interferogram with respect to the zero path difference (ZPD) at $n=n_{zpd}$, i.e.,

$$I_w(n) = w(n)I_m(n), \quad (2)$$

and

$$w(n) = 0.54 - 0.46\cos\left(\frac{2\pi n}{W-1}\right), \left|n - n_{zpd}\right| \le \frac{W-1}{2}, \quad (3)$$

where W is the odd-numbered window length. The windowed interferogram $I_w(n)$ is circular shifted to obtained $I'_w(n)$ such that $I'_w(0)=I_w(n_{zpd})$. The estimated phase function can be derived from the spectral phase response of the windowed interferogram, which is given by

$$N'_w(\sigma) = F\left\{I'_w(n)\right\}, \quad (4)$$

$$\hat{\phi}(\sigma) = \tan^{-1}\frac{\mathrm{Im}(N'_w(\sigma))}{\mathrm{Re}(N'_w(\sigma))}, \quad (5)$$

where $F\{.\}$ denotes the Fourier transform operation. Next, we apply the estimated phase function to the complex spectrum:

* Corresponding author.

$$\hat{N}(\sigma) = N_m(\sigma)e^{-j\hat{\phi}(\sigma)} = N(\sigma)e^{j(\phi(\sigma)-\hat{\phi}(\sigma))} + n(\sigma)e^{-j\hat{\phi}(\sigma)}. \quad (6)$$

The resulting real and imaginary parts of the spectrum are

$$\begin{aligned} \mathrm{Re}\{\hat{N}(\sigma)\} &= N(\sigma) + \mathrm{Re}\{n(\sigma)\}\cos(\hat{\phi}(\sigma)) \\ \mathrm{Im}\{\hat{N}(\sigma)\} &= \mathrm{Im}\{n(\sigma)\}\sin(\hat{\phi}(\sigma)). \end{aligned} \quad (7)$$

Note that the imaginary part contains only the noise component of the uncorrected spectrum in Equation (7).

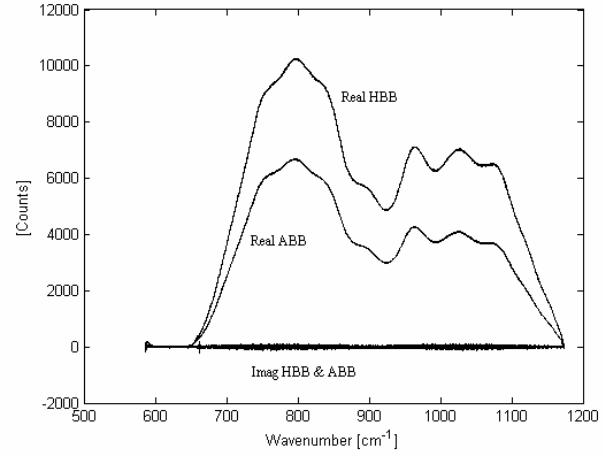

(a)

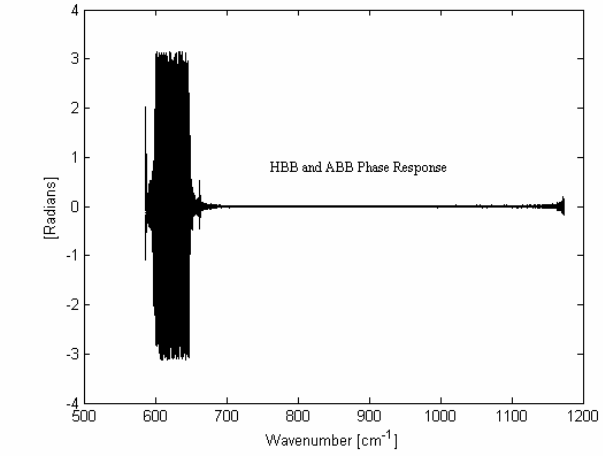

(b)

Figure 1. LW spectral responses after the phase correction for Pixel (64, 65): (a) real and imaginary spectra for HBB (286K) and ABB (260K), and (b) phase responses for HBB and ABB.

Figure 1 depicts the spectral response functions after the phase correction procedure for a LW pixel element over 25 scans. In Figure 1(a), the real and imaginary spectra are shown. Note that the imaginary spectra contain only noise after the correction. Figure 1(b) illustrates the phase responses for HBB and ABB; here the mean phase responses within the spectral band of interest are approximately zero.

The phase correction operation is performed on a set of interferogram scans for the scene measurements and internal blackbody calibration references at ambient and hot temperatures. The resulting real spectra can be written as $N_i^H(\sigma)$, $N_i^A(\sigma)$, and $N_i^S(\sigma)$ for HBB, ABB, and scene, respectively, where *i* denotes the scan number.

2.2 Calibration Procedures

In the calibration stage, the spectral responsivity, based on the previous results and ideal Planck blackbody spectra at given temperatures, can be computed from

$$R(\sigma) = \frac{\overline{N}^H(\sigma) - \overline{N}^A(\sigma)}{B^H(\sigma) - B^A(\sigma)}, \quad (8)$$

in which,

$$\overline{N}^H(\sigma) = \frac{1}{S}\sum_{i=1}^{S} N_i^H(\sigma) \text{ and } \overline{N}^A(\sigma) = \frac{1}{S}\sum_{i=1}^{S} N_i^A(\sigma) \quad (9)$$

represent the mean HBB and ABB spectra over S scans, respectively. Using the relation of

$$\overline{N}^H(\sigma) = R(\sigma)(B^H(\sigma) + O(\sigma)), \quad (10)$$

The offset term can be solved by

$$O(\sigma) = \frac{\overline{N}^A(\sigma)B^H(\sigma) - \overline{N}^H(\sigma)B^A(\sigma)}{\overline{N}^H(\sigma) - \overline{N}^A(\sigma)}. \quad (11)$$

The calibrated HBB, ABB, and scene spectra, therefore, can be determined from

$$\hat{B}_i^H(\sigma) = \frac{N_i^H(\sigma)}{R(\sigma)} - O(\sigma) \quad (12)$$

$$\hat{B}_i^A(\sigma) = \frac{N_i^A(\sigma)}{R(\sigma)} - O(\sigma) \quad (13)$$

$$\hat{N}_i^S(\sigma) = \frac{N_i^S(\sigma)}{R(\sigma)} - O(\sigma) \quad (14)$$

respectively, for *i=1,2,…,S.* Figure 2 illustrates the LW HBB, ABB, and scene spectra obtained from the calibration procedure.

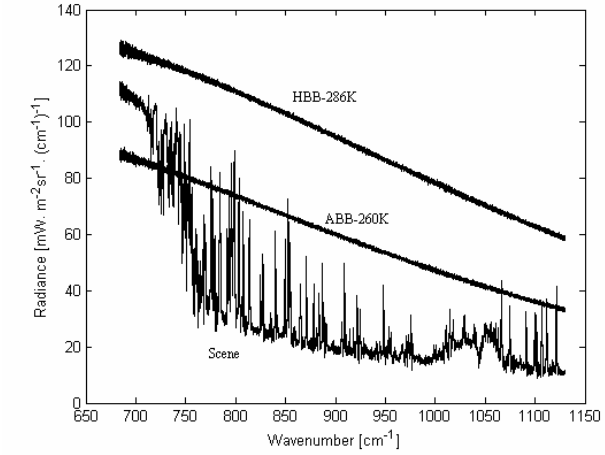

Figure 2. The calibrated LW HBB, ABB, and scene spectra for Pixel (64, 65) over 25 scans.

2.3 Post-calibration Procedures

In the post-calibration stage, the Noise Equivalent Spectral Radiance (NESR) can be estimated from the calibrated ABB and HBB spectra. The NESR is generally considered as a measure of the instrument noise performance, and can be estimated as the standard deviation of calibrated radiance spectra from multiple scans. The definitions for NESRs are given in Equations (15) and (16). Figure 3 shows the smoothed HBB and ABB NESR estimates over 25 scans for a single pixel.

$$NESR^H(\sigma) = \sqrt{\frac{1}{s}\sum_{i=1}^{S}\left(\hat{B}_i^H(\sigma) - \overline{\hat{B}}^H(\sigma)\right)^2} \tag{15}$$

$$NESR^A(\sigma) = \sqrt{\frac{1}{s}\sum_{i=1}^{S}\left(\hat{B}_i^A(\sigma) - \overline{\hat{B}}^A(\sigma)\right)^2} \tag{16}$$

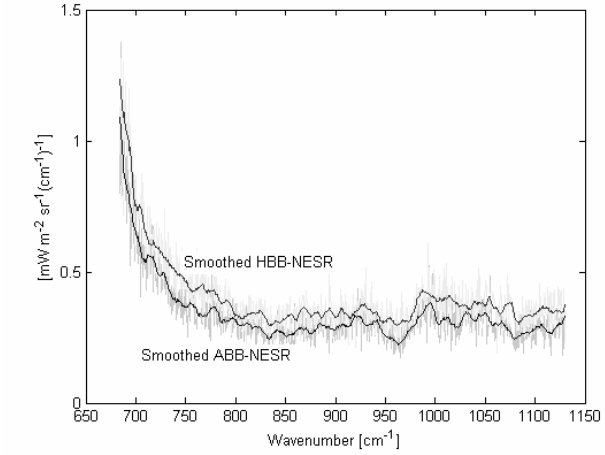

Figure 3. The smoothed LW NESR estimates for HBB and ABB (Pixel (64, 65), 25 scans).

Since the calibration results described in Section 2.2 were obtained based on internal blackbody references, it is necessary to implement a correction scheme that compensates for the effects of fore-optics. This task can be achieved by using additional data measurements collected from an extended source. Given $\overline{C}_e^H(\sigma)$ and $\overline{C}_e^A(\sigma)$ as the calibrated extended blackbody sources averaged over all scans at hot and ambient temperatures, respectively, we have

$$\overline{C}_e^H(\sigma) = R_e(\sigma)B_e^H(\sigma) + O_e(\sigma), \tag{17}$$

$$\overline{C}_e^A(\sigma) = R_e(\sigma)B_e^A(\sigma) + O_e(\sigma). \tag{18}$$

By solving $R_e(\sigma)$ and $O_e(\sigma)$, the actual scene radiances can be approximated as

$$\tilde{N}_i^S(\sigma) = \frac{\hat{N}_i^S(\sigma) - O_e(\sigma)}{R_e(\sigma)}. \tag{19}$$

Figure 4 shows the calibrated LW radiance spectrum before and after performing the fore-optic effect correction procedure.

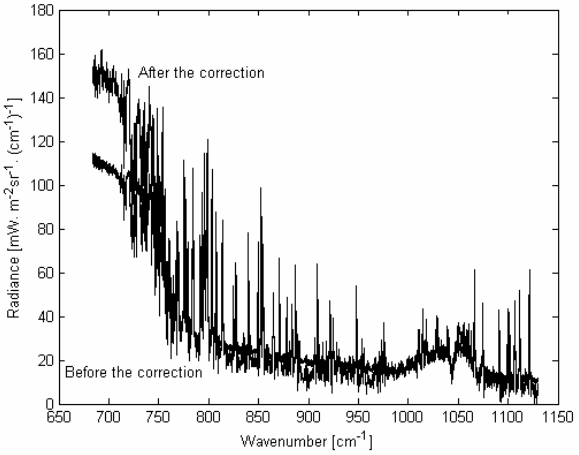

Figure 4. The calibrated LW scene spectrum before and after the fore-optic effect correction.

The final step in the post-calibration process involves the correction of the FPA off-axis effect. Since the GIFTS FPAs contain 128x128 detector elements, the distortion caused by the off-axis effect is too great to be neglected. The off-axis pixels are sampled at slightly shorter optical path differences (OPDs), which cause the spectra of these off-axis pixels to expand to higher wavenumbers (Kauppinen, 2001). The off-axis correction can be formulated as a fractional sampling rate conversion rate problem, which can be solved via sinc interpolations, i.e.,

$$N_i^S(\sigma) = \sum_{m=0}^{M-1} \tilde{N}_i^S(\sigma')\mathrm{sinc}(\sigma - \sigma'), \quad \sigma' = \frac{\sigma}{f}, \tag{20}$$

where σ is the on-axis wavenumber scale, σ' is the off-axis scale, and f is the off-axis factor that can be obtained from the FPA geometry. However, the sinc interpolation method is computational intensive, furthermore, the truncation window associated with the sinc kernels may cause overshoot in the resulting data. It has been shown that the zero-padding interpolation in the interferogram domain is equivalent to the sinc interpolation in the spectral domain except that the zero-padding method cannot be evaluated at an arbitrary point (La Rivière, 1998). To overcome this limitation, we designed the method of "over-padding", in which, we assign an over-padding factor *g* that is closely associated with the final resolution of the corrected spectrum. By over-padding the interferogram *g* times, a fractional sample rate conversion can be realized. For instance, if *f=0.9977*, and the length of the spectrum is *N*, then the zero-padded interferogram length is the round off of *g*N/f*. If *g=100*, the actual off-axis factor of *0.997702* is obtained; if *g=1*, then the actual value of *f* becomes *0.99758* due to round off errors. The corrected spectrum can be obtained by downsampling the Fourier transform of the over-padded interferogram by the factor *g*. Figure 5(a) depicts the calibrated radiance spectra for two LW pixels before any off-axis effect correction was performed. One pixel is located near the center of the FPA while the other is situated near the corner of the FPA. The wavenumber shift can be seen between the two spectra, especially for higher wavenumbers. In Figure 5(b), the corrected spectra for these two pixels are shown. An over-padding factor of *g=20* was assigned during the correction. As a result, a more accurate alignment was achieved between these two spectra.

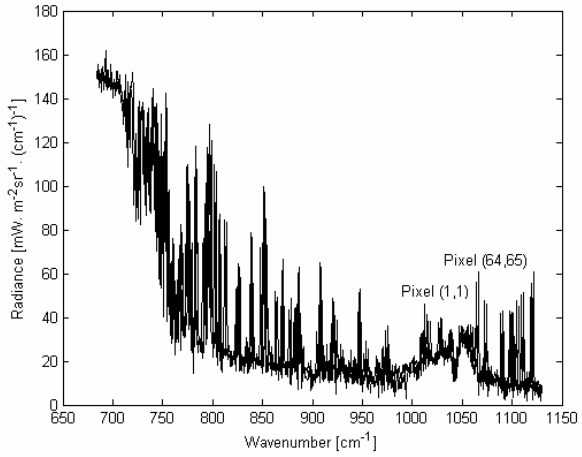

(a)

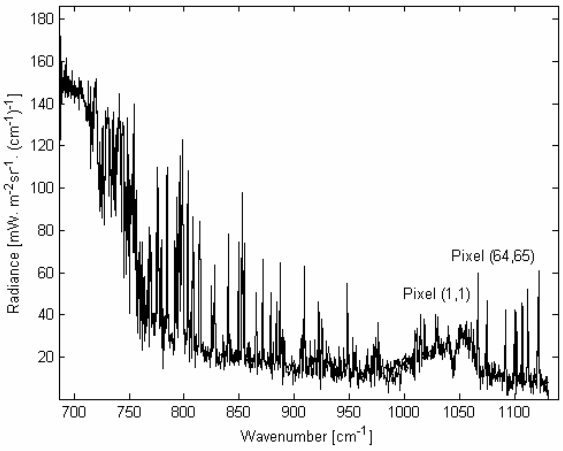

(b)

Figure 5. The off-axis effect correction: (a) center and corner pixels before the off-axis correction, and (b) center and corner pixels after the off-axis correction with the over-padding factor set to 20.

3. CONCLUSIONS

This paper describes the three stages for calibrating the GIFTS SM EDU data spectrally and radiometrically. The first stage involves correcting the complex interferogram for its phase errors via the FVS algorithm. In the second stage, the spectral responsivity is computed, followed by the derivation of calibrated radiance spectra for HBB, ABB, and scene. In the last stage, the NESRs are estimated based on the results from the previous stages. We then compensate for the fore-optic effects using an extended source as the reference. A correction method for the off-axis effect is also presented.

REFERENCES

F. A. Best *et al*., "Calibration of the Geostationary Fourier Transform Spectrometer (GIFTS)," *Proceedings of SPIE*, vol. 4151, pp. 21-31, 2001.

M. L. Forman, W. H. Steel, and G. A. Vanasse, "Correction of asymmetric interferograms obtained in Fourier transform spectroscopy," *J. Opt. Soc. Amer.,* Vol. 56, pp. 59-63, 1966.

J. Kauppinen and J. Partanen, *Fourier Transforms in Spectroscopy*. Berlin, Germany: WILEY-VCH, 2001.

P. J. La Rivière and X. Pan, "Mathematical equivalence of zero-padding interpolation and circular sampling theorem interpolation with implications for direct Fourier image reconstruction," *SPIE Conference on Image Processing*, vol. 3338, pp. 1117-1126, 1998.